Available online at www.sciencedirect.com

ScienceDirect

Physics Procedia 56 (2014) 108 – 116

Physics Procedia

8th International Conference on Photonic Technologies LANE 2014

Selective laser melting additive manufacturing of TiC/AlSi10Mg bulk-form nanocomposites with tailored microstructures and properties

Dongdong Gu[a,b,*], Hongqiao Wang[a,b], Fei Chang[a,b], Donghua Dai[a,b], Pengpeng Yuan[a,b], Yves-Christian Hagedorn[c], Wilhelm Meiners[c]

[a]*College of Materials Science and Technology, Nanjing University of Aeronautics and Astronautics, Yudao Street 29, 210016 Nanjing, People's Republic of China*

[b]*Institute of Additive Manufacturing (3D Printing), Nanjing University of Aeronautics and Astronautics, Yudao Street 29, 210016 Nanjing, PR China*

[c]*Fraunhofer Institute for Laser Technology ILT/Chair for Laser Technology LLT, RWTH Aachen, Steinbachstraße 15, D-52074 Aachen, Germany*

Abstract

The nanoscale TiC particle reinforced AlSi10Mg nanocomposite parts were produced by selective laser melting (SLM) additive manufacturing process. The influence of laser energy density (LED) on densification behavior, microstructural evolution, microhardness and wear properties of SLM-processed TiC/AlSi10Mg nanocomposites was studied. It showed that the near fully dense nanocomposite parts (>98% theoretical density) were achieved with increasing the applied LED. The TiC reinforcement in SLM-processed parts experienced a microstructural change from the standard nanoscale particle morphology (the average size 77-93 nm) to the relatively coarsened submicron structure (the mean particle size 154 nm) as the LED increased. The sufficiently high densification rate combined with the homogeneous distribution of nanoscale TiC reinforcement throughout the matrix led to a high microhardness of 181.2 $HV_{0.2}$, a considerably low coefficient of friction (COF) of 0.36, and a reduced wear rate of 2.94×10^{-5} $mm^3N^{-1}m^{-1}$ for SLM-processed TiC/AlSi10Mg nanocomposite parts.

Peer-review under responsibility of the Bayerisches Laserzentrum GmbH

Keywords: Additive manufacturing; Selective laser melting (SLM); Nanocomposites; Aluminum matrix composites; Wear

* Corresponding author. Tel.: +86-25-52112626; fax: +86-25-52112626 .
E-mail address: dongdonggu@nuaa.edu.cn

Peer-review under responsibility of the Bayerisches Laserzentrum GmbH
doi:10.1016/j.phpro.2014.08.153

1. Introduction

Selective Laser Melting (SLM), as a newly developed freeform fabrication technology, has been regarded as one of the most effective powder-based additive manufacturing (AM) methods for metal parts [Gu et al. (2012), Kruth et al. (2007), Wu et al. (2007)]. According to the computer-aided design (CAD) models of the parts to be created by SLM, the three-dimensional (3D) parts are built by selectively fusing and consolidation of the thin layers of powder using the high-energy laser beam in a layer-by-layer manner [Song et al. (2014), Zhang et al. (2013), Hagedorn et al. (2010), Yadroitsev et al. (2007)]. Due to the unique processing mechanisms of SLM, i.e., a full melting of powder materials followed by a rapid solidification, the molten materials tend to experience a significantly non-equilibrium metallurgical process during SLM process, thereby providing a capacity to produce novel materials with unique microstructural features and mechanical performance.

In recent years, there is an increasing demand for the lightweight materials with high strength and stiffness in modern industries [Tjong et al. (2007)]. Particle reinforced aluminum matrix composites (AMCs), because of its low density, high strength, low coefficient of thermal expansion, and outstanding abrasion resistance, can meet these requirements. AMCs accordingly have been widely used in the industrial fields of aerospace, automotive, microelectronics, etc. For the conventional AMCs, the relatively large sized ceramic reinforcing particles in the range of several ten micrometers to several hundred micrometers are normally used. However, due to the limited interfacial wetting characteristics between ceramics and metals, the large ceramic particles are prone to cracking during mechanical loading, resulting in the poor ductility and premature failure of AMCs [Tjong et al. (2007)]. It has been revealed that both tensile strength and ductility of AMCs increase with lowering the particle size of the reinforcement. Therefore, the application of the refined ceramic reinforcing particles can efficiently improve the mechanical properties of AMCs. Previous studies have confirmed that the mechanical properties of AMCs can be further enhanced by decreasing the size of ceramic reinforcing particles from micrometer to nanometer levels [Gu et al. (2011)]. Such materials are known as nanocomposites. Nevertheless, it is rather difficult to achieve a uniform/regular distribution of nanoscale reinforcement throughout metal matrix. Because of the extremely large van der Waals attractive force between adjacent nanoparticles, the nanoparticles tend to agglomerate into the coarsened clusters, resulting in the microstructural inhomogeneity. Therefore, it is urgent to find a novel processing method to avoid particulate aggregation and, accordingly, homogenize the nanoparticles throughout the matrix.

The previous studies have shown that SLM processing of aluminium alloys is much more difficult than titanium alloys, nickel alloys or steels [Sun et al. (2011), Simchi et al. (2004)]. This is mainly attributed to the unique physical properties of the aluminum powder including (i) the considerably low absorptivity (only 9%) of the aluminum powder to the laser beam, (ii) the high heat conductivity of 237 W/(mK) that is eleven-fold compared to Ti and five-fold compared to Fe; and (iii) the high affinity to oxygen and elevated oxidation kinetics [Olakanmi et al. (2013), Louvis et al. (2011)]. Fortunately, the aluminium alloy parts with densities exceeding 97% can be produced successfully via SLM process, typically using the casting alloy AlSi10Mg as the starting powder [Brandl et al. (2012), Kempen et al. (2012), Buchbinder et al. (2011)]. In the present work, the material as investigated was broadened from the conventional AlSi10Mg alloy to the nanocrystalline TiC reinforced AlSi10Mg based nanocomposites. The bulk-form TiC/AlSi10Mg nanocomposites with the uniformly distributed nanoscale reinforcement were successfully prepared by SLM process. The microstructural evolution of nanoscale reinforcement in SLM-processed parts at different laser processing parameters was studied and the attendant densification level and wear property were assessed. A material-microstructure-property relationship was established to enable the successful production of AMCs parts with nanoscale reinforcement architecture and elevated mechanical performance.

2. Experimental procedures

2.1. Powder preparation

The 99.7% purity AlSi10Mg powder with a spherical shape and an average particle diameter of 30 μm (Fig. 1a) and the 99.0% purity TiC nanopowder with a near spherical shape and a mean particle size of 50 nm (Fig. 1b) were used. The TiC and AlSi10Mg powder components consisting of 5 wt.% TiC were mechanically mixed in a

Pulverisette 4 vario-planetary mill (Fritsch GmbH, Germany), using a ball-to-powder weight ratio of 1:1, a rotation speed of main disk of 200 rpm, and a mixing duration of 4 h. After ball milling, the AlSi10Mg powder well maintained its spherical shape and, meanwhile, the TiC nanoparticles were dispersed uniformly around the surface of AlSi10Mg particles, leading to the favorable flowability of the mixed TiC/AlSi10Mg nanocomposite powder system.

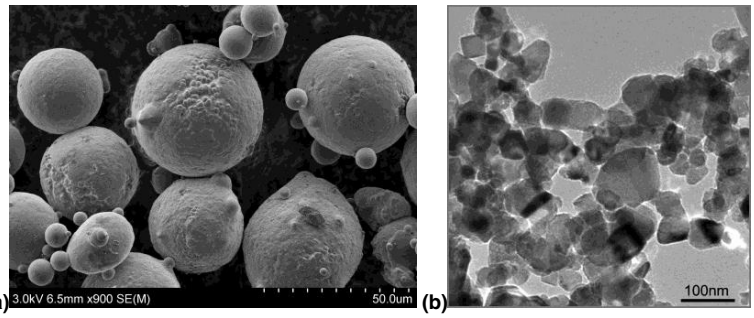

Fig. 1. Typical particle morphology of the starting AlSi10Mg powder (a) and nanoscale TiC powder (b).

2.2. SLM process

The SLM system, as schematically depicted in Fig. 2a, consisted mainly of a YLR-200-SM ytterbium fiber laser with a power of ~200 W and a spot size of 70 μm (IPG Laser GmbH, Germany), an automatic powder spreading device, an inert argon gas protection system, and a computer system for process control. As the specimens were to be built, an aluminium substrate was fixed on the building platform and levelled. The building chamber was then sealed and the argon gas with an outlet pressure of 30 mbar was fed inside, decreasing the O_2 content below 20 ppm. Afterwards, the nanocomposite powder was deposited on the substrate by the layering mechanism, with a powder layer thickness of 50 μm. The laser beam was then controlled by the CAD data to scan the powder bed surface selectively, forming a two-dimensional profile. A simple linear raster scan pattern was used, with a scan vector length of 4 mm and a hatch spacing of 50 μm. The laser power (P) was optimized at 110 W and the scan speeds (v) were set at 100, 150, 250, and 350 mm/s by the SLM control program, in order to change the processing conditions during experiments. Four different "laser energy densities" (LED) of 1100, 733, 440, 314 J/m, which were defined by LED=P/v, were used to assess the laser energy input to the powder layer being processed [Gu et al. (2009)]. The rectangular specimens with dimensions of 20 mm ×10 mm ×5 mm were built in a layer-by-layer manner until completion, as shown in Fig. 2b.

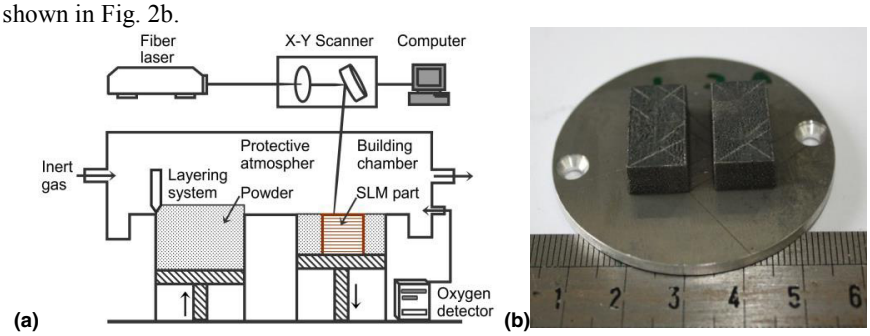

Fig. 2. Schematic of SLM apparatus (a) and photograph of SLM-processed TiC/AlSi10Mg nanocomposite parts (b).

2.3. Microstructural characterization and mechanical properties testing

Specimens for metallographic examinations were prepared according to the standard procedures, and etched with a solution composing HF (2 ml), HCl (3 ml), HNO_3 (5 ml) and distilled water (190 ml) for 10 s. A PMG3 optical

microscope (OM) (Olympus Corporation, Japan) was used to observe the low-magnification microstructures of SLM-processed specimens. High-resolution study of the ultrafine nanostructures was performed using a S-4800 field emission SEM (FE-SEM) (Hitachi, Japan) at 5 kV. Chemical compositions were determined by an EDAX energy dispersive X-ray spectroscope (EDX) (EDAX Inc., USA). The Archimedes principle was used to measure the density (ρ) of the specimens. The Vickers hardness was measured using a MicroMet 5101 microhardness tester (Buehler GmbH, Germany) at a load of 0.2 kg and an indentation time of 20 s. The wear property of specimens was estimated by the dry sliding wear tests conducted in a HT-500 ball-on-disk tribometer (Lanzhou ZhongKe KaiHua Sci. &Technol. Co., Ltd., China) in air at room temperature. The counter material was GCr15 bearing steel ball with a diameter of 3 mm and a mean hardness of HRC60, using a test load of 3 N was applied. The friction unit was rotated at a speed of 560 rpm for 15 min, with the rotation radius of 2 mm. The coefficient of friction (COF) of the specimens was recorded during wear tests. The wear volume (V) was determined gravimetrically using $V=M_{loss}/\rho$, where M_{loss} was the weight loss of the specimens after wear tests. The wear rate (ω) was calculated by $\omega=V/(WL)$, where W was the contact load and L was the sliding distance.

3. Results and discussion

3.1. Densification behavior

The influence of laser energy input on the cross-sectional microstructures and densification behavior of SLM-processed TiC/AlSi10Mg nanocomposite parts were given in Fig. 3. Upon etching, the layerwise microstructure features became visible, due to the additive manufacturing nature of SLM. At a relatively low LED of 314 J/m, the cross-section of SLM parts showed a relatively heterogeneous layerwise microstructure with the formation of the irregular shaped inter-layer pores on a scale of several tens of micrometers (Fig. 3a). The corresponding densification rate was about 91.7% theoretical density (TD). FE-SEM characterization revealed that there were a large amount of metallic balls with the diameters of several tens of micrometers formed on the SLM-processed surface (Fig. 3e). It was accordingly concluded that the balling effect, which was a typical metallurgical defect associated with powder bed based SLM process [Gu et al. (2012), Kruth et al. (2007)], initiated in this instance. As the LED increased to 440 J/m, although a small amount of inter-layer micro-cracks were still present on the cross-section (Fig. 3b), the relative density of the SLM-processed part increased apparently to 95.0% TD. When the LED further increased above 733 J/m, the cross-section showed a homogeneous microstructure with the evenly distributed layers, showing the coherent interlayer bonding ability free of any residual pores or cracks (Fig. 3c and d). In these situations, the near fully dense (>98% TD) TiC/AlSi10Mg parts were generally produced after SLM.

During SLM, the TiC/AlSi10Mg nanocomposite powder is melted line-by-line by the laser beam, forming a mobile molten pool with a continuous liquid front. The amount of the liquid formed in the molten pool influences the densification and the resultant microstructure of the SLM-processed parts by changing the thermokinetic and thermocapillary characteristics such as viscosity, wettability, and liquid-solid rheological properties. For the TiC/AlSi10Mg system being investigated, the presence of TiC reinforcing particles in aluminum alloy liquid tends to increase the viscosity of the melt significantly, hence handicapping the sufficient flow of the melt and decreasing the overall rheological performance of the composite melt. Meanwhile, using a lower LED results in a limited SLM temperature and, accordingly, further elevates the viscosity of the melt [Simchi et al. (2004)]. The combined influence of the material nature and the insufficient laser energy input below 440 J/m tends to reduce the wettability of the melt within the pool, hence decreasing the densification response after solidification of the melt. Furthermore, during high-energy laser scanning, a steep temperature gradient is developed between the center and edge of the pool across the surface, giving rise to surface tension gradients and resultant Marangoni convention. Due to the action of Marangoni flow, the melt tends to flow radially inward towards the melt pool center, instead of spreading outward on the underlying surface [Niu et al. (1999)]. Consequently, the instable melt track breaks up into several spherical agglomerates to achieve the equilibrium state, which is termed as “balling” effect. During layer-by-layer SLM process, balling effect is detrimental to the uniform deposition of the fresh powder on the previously processed layer. As the laser beam scans over such an uneven powder layer, especially at a high scan speed (i.e., a low LED), the melting/solidification front of the moving molten pool undergoes a significant disturbance and even interruption, causing the residual pores between the uneven SLM layers and the limited densification response after solidification

(Fig. 3a and b). Therefore, the high melt viscosity and limited wetting characteristics caused by an insufficient laser energy input are the key factors in producing balling effect and interlayer pores, hence weakening the densification activity of SLM-processed TiC/AlSi10Mg nanocomposite parts.

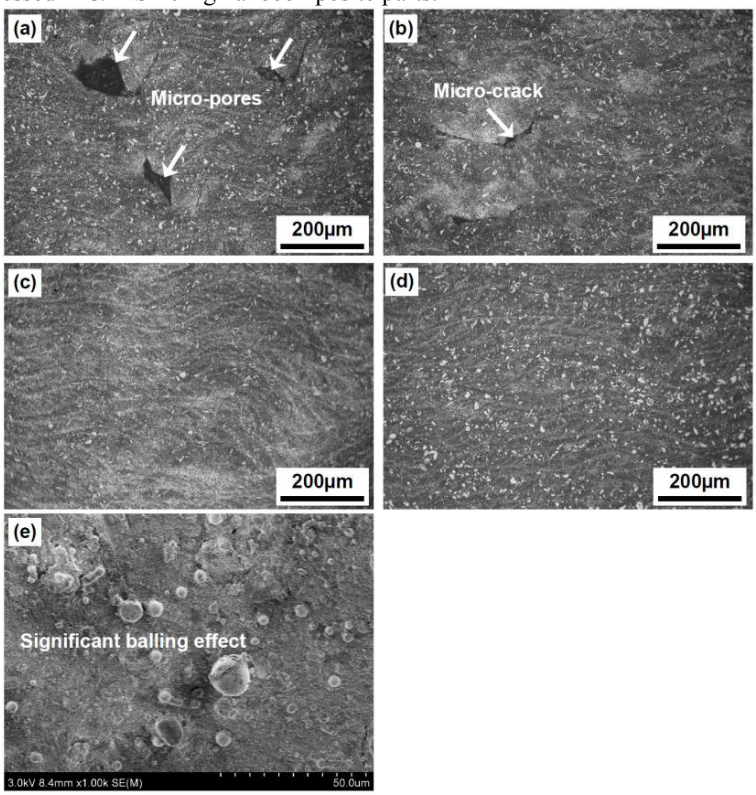

Fig. 3. OM images showing characteristic microstructures on cross-sections of SLM-processed TiC/AlSi10Mg nanocomposite parts at different LED: (a) 314 J/m; (b) 440 J/m; (c) 733 J/m; (d) 1100 J/m. Surface morphology of SLM-processed part at a low LED of 314 J/m showing the occurrence of balling effect (e).

3.2. Microstructural evolution

Fig. 4a-d illustrates the typical microstructures of SLM-processed TiC/AlSi10Mg nanocomposite parts. The mean sizes of TiC reinforcing particles are measured and calculated during SEM analysis and the quantitative determination of the corresponding average particle size of reinforcement is depicted in Fig. 4e. The quantitative EDX elemental analysis elucidated that the chemical compositions of reinforcement formed at various LEDs were Ti and C elements with the atomic ratio very close to 1:1. It was accordingly reasonable to consider that the reinforcement in SLM-processed nanocomposites was stoichiometric TiC. Although the TiC reinforcement had similar microstructure to the starting particulate morphology before SLM, its dispersion state and particle size were significantly influenced by the applied LED. At a relatively low LED of 314 J/m, the ultrafine TiC reinforcing particles with a mean size of 77 nm were formed (Fig. 4a and e). However, the nanostructured TiC reinforcement showed a high tendency to aggregate into clusters, resulting in the formation of micron-sized agglomerates which consisted of several nanoparticles, as selectively indicated in Fig. 4a. As LED increased to 440 J/m, the FE-SEM characterization revealed that the distribution state of TiC reinforcing particles was improved (Fig. 4b). The average particle size of TiC reinforcement slightly increased to 80 nm in this instance (Fig. 4e). With a further increase in LED to 733 J/m, a uniform distribution of the TiC reinforcement throughout the matrix was obtained and there was no apparent aggregation of TiC nanoparticles in a microscopic scale within SLM-processed structure (Fig. 4c). The

average size of TiC reinforcing particles, 93 nm, was well within the nanometer scale (Fig. 4e). At an even higher LED of 1100 J/m, although the uniform distribution state of TiC reinforcement was still maintained (Fig. 4d), the mean particle size of TiC reinforcement increased markedly to 154 nm (Fig. 4e), which indicated that the TiC reinforcement lost its favorable nanostructure after SLM process. It was accordingly concluded that the microstructural development of the nanoscale TiC reinforcement during SLM was sensitive to the laser energy input.

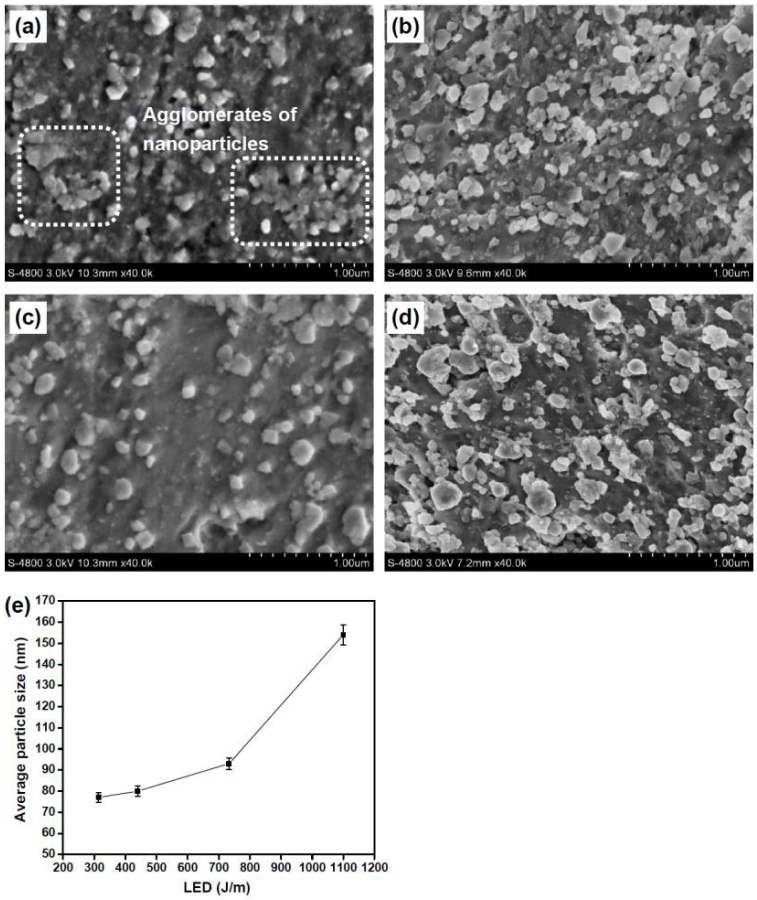

Fig. 4. FE-SEM showing dispersion states and characteristic morphologies of TiC reinforcement in SLM-processed TiC/AlSi10Mg nanocomposite parts at various LED: (a) 314 J/m; (b) 440 J/m; (c) 733 J/m; (d) 1100 J/m. Change of the average particle size of TiC reinforcement with the applied LED of 314, 440, 733 and 1100 J/m (e).

Typically, laser melting offers a high heating/cooling rate, contributing to the development of the nanostructured TiC reinforcement by shortening growth time for TiC grains. In the present study, it is found that a reasonable increase in the applied LED from 314 J/m to 733 J/m can homogenize the dispersion state of the nanoscale TiC reinforcing particles; however, an excessive laser energy input at 1100 J/m resulted in the significant coarsening of TiC grains and attendant disappearance of the nanostructure of the reinforcement. On one hand, the formation of the Marangoni convention within the molten pool tends to induce the liquid capillary force, which in turn acts on the TiC reinforcing particles and promotes its rearrangement in the pool. As a relatively high LED is applied, the significantly enhanced SLM temperature intensifies the Marangoni flow in the molten pool and the attendant magnitude of capillary force [Niu et al. (1999), Zhong et al. (2010)]. Consequently, the rearrangement rate of the nanoscale TiC reinforcing particles in the melt is elevated, thereby avoiding the aggregation of TiC nanoparticles and homogenizing their dispersion state throughout the finally solidified matrix (Fig. 4c). On the other hand, the

laser energy input influences the microstructural evolution of the nanoscale TiC reinforcement by changing the operative undercooling degree and attendant solidification rate. With the increase of the applied LED, the thermalization of laser energy is elevated, resulting in a significant thermal accumulation and a higher SLM temperature within the molten pool. In this situation, the effect of quenching that occurs by conduction of heat through the substrate is not significant. The activity of the grains within the nanoscale TiC reinforcing particles becomes significantly elevated in the molten pool having a slower cooling rate and, accordingly, the TiC grains tend to experience a rapid growth. As a result, the TiC grains become coarsened continuously as the applied LED increases above 1100 J/m and eventually the TiC reinforcing particles lose the initial standard nanostructure after SLM (Fig. 4d and e).

3.3. Hardness and wear properties

Fig. 5a depicts the average microhardness measured on the cross-sections of SLM-processed TiC/AlSi10Mg nanocomposite parts. With the increase of the applied LED from 314 J/m to 733 J/m, the average microhardness experienced a continuous increase from 158.7 $HV_{0.2}$ to 181.2 $HV_{0.2}$; however, as the LED further increased to 1100 J/m, the mean microharness decreased to 173.8 $HV_{0.2}$. Therefore, the microhardness of the TiC/AlSi10Mg part was considerably improved by increasing the LED to 700 J/m, due to the homogeneous incorporation of nanoscale TiC reinforcing particles throughout the matrix (Fig. 4c and e). However, a further enhancement of the applied LED to 1100 J/m did not lead to a further elevation of the obtainable microhardness, which indicated that the significant grain coarsening and the resultant disappearance of nanostructured TiC reinforcement (Fig. 4d and e) tended to lower the hardness performance. Nevertheless, a close comparison revealed that the SLM-processed AlSi10Mg parts reinforced with nanoscale TiC particles, for all the given SLM parameters, demonstrated the superior hardness compared to the unreinforced AlSi10Mg parts fabricated with the same SLM conditions (maximum at approx. 145 $HV_{0.1}$) [Buchbinder et al. (2011)].

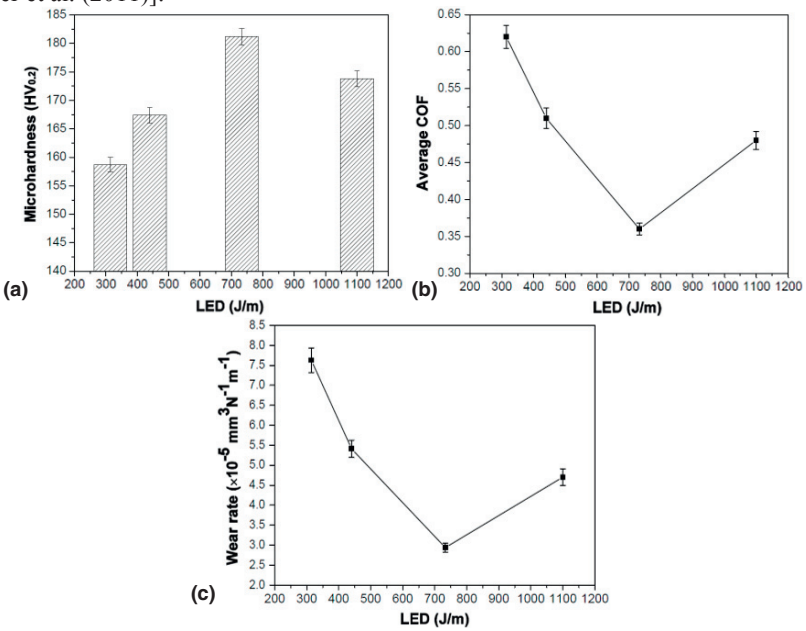

Fig. 5. Microhardness (a), average COF values (b) and wear rates (c) of SLM-processed TiC/AlSi10Mg nanocomposite parts using different LED of 314, 440, 733 and 1100 J/m.

Fig. 5b and c shows the influence of SLM parameters on COFs and wear rates of SLM-processed TiC/AlSi10Mg nanocomposite parts. The FE-SEM studies of the corresponding worn surfaces are provided in Fig. 6. The large differences in COF values and attendant wear rates among various parts indicated that the wear performance of

SLM-processed parts was significantly influenced by the applied laser processing conditions. At a relatively low LED of 314 J/m, the average COF reached a high value of 0.62 (Fig. 5b), resulting in a considerably elevated wear rate of 7.63×10^{-5} $mm^3N^{-1}m^{-1}$ (Fig. 5c). The wear surface was disruptive and consisted of large-sized agglomerates which contained some ultrafine nanoscale particles (Fig. 6a). The presence of irregular shaped fragments revealed the local severe deformation and delamination of the worn surface occurred. On increasing the LED to 440 J/m, the mean COF and attendant wear rate decreased to 0.51 (Fig. 5b) and 5.42×10^{-5} $mm^3N^{-1}m^{-1}$ (Fig. 5c), respectively. Interestingly, at a reasonable LED of 733 J/m, the worn surface of SLM-processed sample became rather smooth and the reinforcing nanoparticles were found to be inserted within the adhesive tribolayer (Fig. 6b). The lowest COF of 0.36 (Fig. 5b) and wear rate of 2.94×10^{-5} $mm^3N^{-1}m^{-1}$ (Fig. 5c) were obtained in this instance. It was accordingly reasonable to consider that as the nanostructured TiC reinforcement with a homogenous dispersion state was formed in SLM-processed parts, the mechanism of material removal during sliding was changed from the abrasion to adhesion of the tribolayer. Such a transition was expected to homogenize the COF values and reduce the wear rate after sliding tests. However, at an even higher LED of 1100 J/m, the parallel, deep grooves were observed on the worn surface (Fig. 6c), which revealed the severe deformation and plowing of the surface during siding. In this situation, the wear mechanism was micro-ploughing rather than the adhesive wear. Some relatively large-sized reinforcing particles were also observed at the edges of grooves on the worn surface. The obtained average COF value of 0.48 (Fig. 5b) and wear rate of 4.70×10^{-5} $mm^3N^{-1}m^{-1}$ (Fig. 5c) showed an apparent increase in this case.

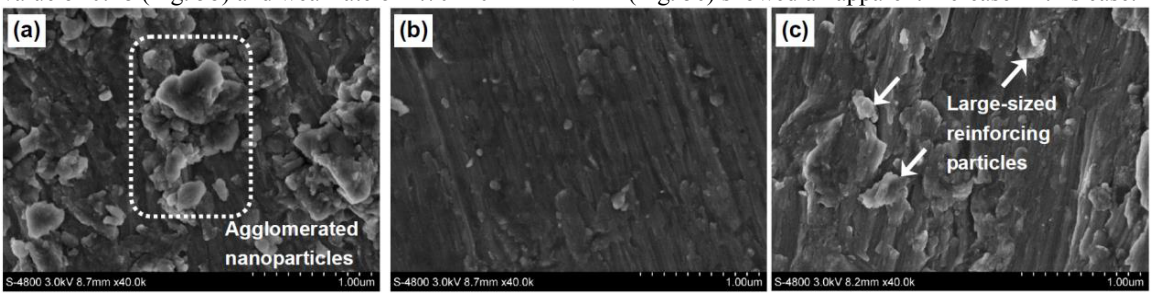

Fig. 6. FE-SEM images showing characteristic morphologies of worn surfaces of SLM-processed TiC/AlSi10Mg nanocomposite parts at: (a) 314 J/m; (b) 733 J/m; (c) 1100 J/m.

4. Conclusions

(1) The densification behavior of TiC/AlSi10Mg nanocomposite parts was significantly affected by the laser energy input during SLM. Using an insufficient LED lowered the SLM densification rate due to the balling effect and the formation of residual pores. The near fully dense nanocomposite parts (>98% theoretical density) were achieved when the suitable LED larger than 733 J/m were properly used.

(2) The TiC reinforcement in SLM-processed TiC/AlSi10Mg nanocomposite parts experienced a structural change from the standard nanoscale particle morphology (the average size of 77-93 nm) to the relatively coarsened submicron structure (the mean particle size of 154 nm) as the LED increased. The nanostructure of TiC reinforcement was successfully maintained within a wide range of LED from 314 to 733 J/m. The dispersion state of nanoscale TiC reinforcement was homogenized from the apparent agglomerates to the uniform distribution with the increase of LED.

(3) The densification rate of SLM-processed TiC/AlSi10Mg nanocomposite parts and the particle morphology and dispersion state of TiC reinforcement in the matrix played the key roles in determining the wear property. The sufficiently high densification rate combined with the uniform distribution of nanoscale TiC reinforcement throughout the matrix led to the considerably low COF of 0.36 and wear rate of 2.94×10^{-5} $mm^3N^{-1}m^{-1}$ for SLM-processed nanocomposites at LED of 733 J/m. The insufficient densification of SLM parts at a relatively low LED and the disappearance of nanoscale reinforcement at a high LED generally lowered the wear performance of TiC/AlSi10Mg nanocomposite parts.

Acknowledgements

We gratefully appreciate the financial support from the National Natural Science Foundation of China (No. 51322509 and No. 51104090), the Outstanding Youth Foundation of Jiangsu Province of China (No. BK20130035), the Program for New Century Excellent Talents in University (No. NCET-13-0854), the Program for Distinguished Talents of Six Domains in Jiangsu Province of China (No. 2013-XCL-028), the Science and Technology Support Program (The Industrial Part), Jiangsu Provincial Department of Science and Technology of China, the Fundamental Research Funds for the Central Universities (No. NE2013103), and the Qing Lan Project, Jiangsu Provincial Department of Education of China.

References

Simchi, A., Pohl, H., 2004. Direct laser sintering of iron–graphite powder mixture. Mater. Sci. Eng. A 383, 191–200.

Brandl, E., Heckenberger, U., Holzinger, V., Buchbinder, D., 2012. Additive manufactured AlSi10Mg samples using Selective Laser Melting (SLM): Microstructure, high cycle fatigue, and fracture behavior. Mater. Design 34, 159–169.

Buchbinder, D., Schleifenbaum, H., Heidrich, S., Meiners, W., Bültmann J., 2011. High Power Selective Laser Melting (HP SLM) of Aluminum Parts. Physics Procedia 12, 271–278.

Gu, D.D., Meiners, W., Wissenbach, K., Poprawe, R., 2012. Laser additive manufacturing of metallic components: materials, processes and mechanisms. Int. Mater. Rev. 57, 133–164.

Gu, D.D., Hagedorn Y.C., Meiners, W., Wissenbach, K., Poprawe, R., 2011. Nanocrystalline TiC reinforced Ti matrix bulk-form nanocomposites by Selective Laser Melting (SLM): Densification, growth mechanism and wear behavior. Compos. Sci. Technol. 71, 1612–1620.

Gu, D.D., Shen, Y.F., 2009. Effects of processing parameters on consolidation and microstructure of W–Cu components by DMLS. J. Alloys Compd. 473, 107–115.

Hagedorn, Y.C., Wilkes, J., Meiners, W., Wissenbach, K., Poprawe, R., 2010. Net shaped high performance oxide ceramic parts by selective laser melting. Physics Procedia 5, 587-594.

Kempen, K., Thijs, L., Van Humbeeck, J., Kruth, J.P., 2012. Mechanical Properties of AlSi10Mg Produced by Selective Laser Melting. Physics Procedia, 39, 439-446.

Kruth, J.P., Levy, G., Klocke, F., Childs, T.H.C., 2007. Consolidation phenomena in laser and powder-bed based layered manufacturing. CIRP Annals – Manuf. Technol. 56, 730–759.

Louvis, E., Fox, P., Sutcliffe, C.J., 2011. Selective laser melting of aluminium components. J. Mater. Process Technol. 211, 275–284.

Niu, H.J., Chang, I.T.H., 1999. Instability of scan tracks of selective laser sintering of high speed steel powder. Scripta Mater. 41, 1229–1234.

Olakanmi, E.O., 2013. Selective laser sintering/melting (SLS/SLM) of pure Al, Al–Mg, and Al–Si powders: Effect of processing conditions and powder properties. J. Mater. Process Technol. 213, 1387–1405.

Song, B., Dong, S., Deng, S., Liao, H., Coddet, C., 2014. Microstructure and tensile properties of iron parts fabricated by selective laser melting. Opt. Laser Technol. 56, 451–460.

Sun, G.F., Bhattacharya, S., Dinda, G.P., Dasgupta, A., Mazumder, J., 2011. Microstructure evolution during laser-aided direct metal deposition of alloy tool steel. Scripta Mater. 64, 454–457.

Tjong, S.C., 2007. Novel nanoparticle-reinforced metal matrix composites with enhanced mechanical properties. Adv. Eng. Mater. 9, 639–652.

Wu, X., 2007. A review of laser fabrication of metallic engineering components and of materials. Mater. Sci. Technol. 23, 631–640.

Yadroitsev, I., Thivillon, L., Bertrand, P., Smurov, I., 2007. Strategy of manufacturing components with designed internal structure by selective laser melting of metallic powder. Appl. Surf. Sci. 254, 980–983.

Zhang, B.C., Liao, H.L., Coddet, C., 2013. Selective laser melting commercially pure Ti under vacuum. Vacuum 95, 25–29.

Zhang, B.C., Dembinski, L., Coddet, C., 2013. The study of the laser parameters and environment variables effect on mechanical properties of high compact parts elaborated by selective laser melting 316L powder. Mater. Sci. Eng. A 584, 21–31.

Zhong, M., Liu, W., 2010. Laser surface cladding: the state of the art and challenges. Proc. Inst. Mech. Eng. Part C: J. Mech. Eng. Sci. 224, 1041–1060.